DOI: 10.1002/adma.200702495

The Patterning of Sub-500 nm Inorganic Oxide Structures**

By *Meredith J. Hampton, Stuart S. Williams, Zhilian Zhou, Janine Nunes, Doo-Hyun Ko, Joseph L. Templeton, Edward T. Samulski,* and *Joseph M. DeSimone**

Replication of sub-micrometer-sized features is a challenging problem in materials science. Over the past few decades, soft lithography, an embossing technique, has emerged as an important tool for low-cost fabrication processes and for pattern replication at micrometer and nanometer length scales.[1] Embossing typically involves the patterning of soft materials such as polymers, organic compounds, and biological molecules into continuous arrays of patterned features using molds that have a high modulus (quartz/glass, glassy polymers) or a low modulus (soft elastomeric materials).[1–3] Until recently, the latter class of materials has been dominated by the elastomer polydimethylsiloxane (PDMS).[4,5] In 2004 Rolland et al. exploited the excellent solvent resistance and the inherent release properties of perfluoropolyether (PFPEs) elastomers as a molding material for soft lithography.[6–7] Herein, we describe the successful application of PFPE molds for patterning inorganic oxides.

Embossing uses either hard or elastomeric molds to generate features that form on top of an interconnecting flash layer. By contrast, Particle (or Pattern) Replication in Non-wetting Templates (PRINT) uses the non-wetting characteristics of PFPE-based elastomers to generate micrometer- and nanometer-scale features that are free of the interconnecting flash layer and can therefore generate arrays of discrete features or populations of discrete particles.[9,10] Flash-free pattern or particle formation is possible because of the exceedingly low surface energy (8–10 dynes cm^{-1}, 1 dyne $= 1 \times 10^{-5}$ N) and high gas permeability of PFPEs.[11] Both attributes of PFPEs enable non-wetting ($\theta_{adv} > 90°$: θ_{adv} = advancing contact angle at the liquid/solid interface) and partially wetting liquids ($0 > \theta_{adv} > 90°$) to fill intricate mold cavities completely through capillary rise or externally applied forces and also allow the removal of excess liquid, as shown in Figure 1. In this study, we explicitly use the low surface energy and high gas permeability of crosslinked PFPE-based materials to showcase the chemical inertness of fluoroelastomers. Additionally, we illustrate the use of aggressive chemistry techniques during the PRINT processes; this enables the formation of uniquely patterned, sub-500 nm-sized inorganic oxide materials with potential applications in photovoltaics, super capacitors, biological sensors and electrodes, and various other electronic and optical devices.[12–18] A range of oxides including TiO_2, SnO_2, ZnO, ITO (Sn-doped indium oxide), and $BaTiO_3$ were formed into arrays with control over size, shape, and composition, both with and without an interconnecting flash layer.

Reports in the literature detail the patterning of sol–gel-derived inorganic oxides using traditional soft-lithography techniques.[19–22] Most notable have been the research efforts of Whitesides and co-workers, who employed PDMS molds and liquid sol–gel precursors in order to replicate surface patterns (down to 1 μm).[23] There have also been reports of features with sizes smaller than 500 nm; these resulted from a significant volume reduction of the sol–gels after calcination using micrometer-sized elastomeric molds.[24,25]

The chemical and physical properties of a PFPE mold provide many advantages over hard imprint methods, such as nanoimprint lithography (NIL) and step-and-flash imprint lithography (SFIL): (i) air-permeable molds allow complete filling; (ii) layer-by-layer deposition can be achieved without destruction of the first layer; (iii) a range of feature sizes can be produced in one step, and (iv) elimination of a residual flash layer avoids the use of harsh reactive-ion etching (RIE) conditions.[24] PRINT offers a versatile patterning method that provides uniformity, size control, multilayer deposition, surface functionalization, and adaptability to various materials.

A schematic representation of the PRINT process is illustrated in Figure 1a–e. A silicon master template with the desired dimensions was fabricated using standard lithographic techniques. A liquid PFPE precursor solution comprising 1000 g mol^{-1} PFPE α,Ω-functionalized dimethacrylate and the photoinitiator 2,2-diethoxyacetophenone was poured over the ''nanopatterned'' master template. The PFPE

[*] Prof. J. M. DeSimone, M. J. Hampton, S. S. Williams, J. Nunes, D.-H. Ko, Prof. J. L. Templeton, Prof. E. T. Samulski
Department of Chemistry
University of North Carolina at Chapel Hill
CB #3290, Caudill Labs, Chapel Hill, NC 27599 (USA)
E-mail: desimone@unc.edu
Prof. J. M. DeSimone
Department of Chemical Engineering
North Carolina State University
Raleigh, NC 27695 (USA)
Dr. Z. Zhou
Liquidia Technologies, P.O. Box 110085
Research Triangle Park, NC 27709 (USA)

[**] M.J.H. and S.S.W. contributed equally to this work. We acknowledge the help of P. White (X-ray diffractometry), David Shirvanyants (image analysis), and Kevin Herlihy (figures). This work was partially supported by the Office of Naval Research, the STC program of the National Science Foundation, NSF (NIRT: Bio-Inspired Actuating Structures CMS-0507151), NASA (URETI ''Biologically Inspired Materials'' Grant NAG-1-2301), the Army Research Office, and the William R. Kenan Jr. Distinguished Professorship.

ADVANCED MATERIALS

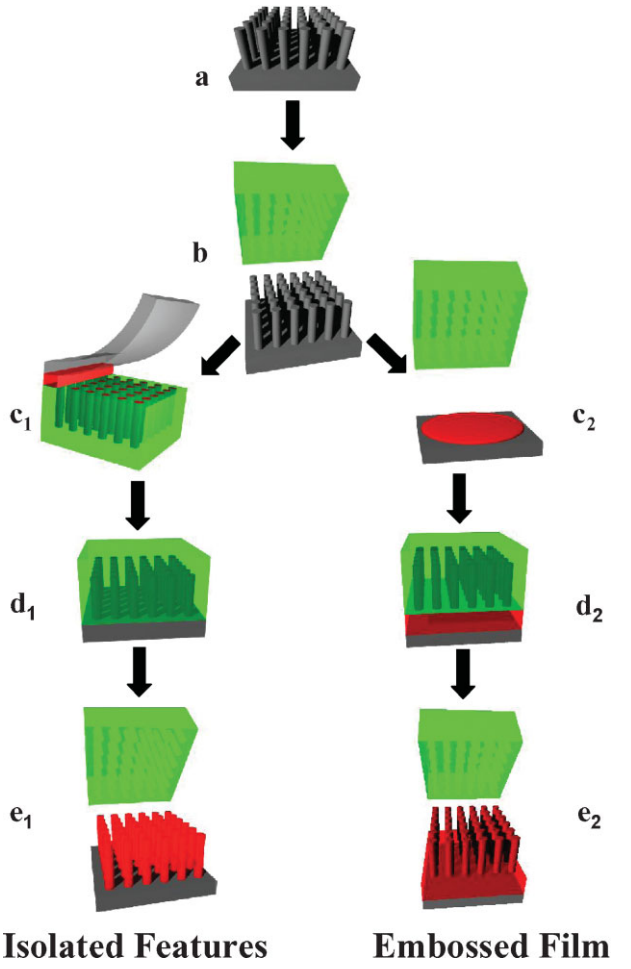

Figure 1. Schematic illustration of the PRINT process: a) Si master template; b) mold release from the master template; c1) mold filling via capillary fill with a poly(ethylene) sheet; d1) pattern transfer to the substrate at elevated temperature and pressure; e1) mold release from the obtained array of isolated features; c2) embossing a liquid precursor; d2) pattern transfer to the substrate at elevated temperature and pressure; e2) mold release from the embossed film.

precursor was then photochemically crosslinked to provide an elastomeric mold of the master template. In order to obtain an array of isolated features (as shown in Figure $1c_1$–e_1), mold cavities were filled with a liquid sol by taking advantage of capillary-fill processes. The sol was dropped onto the mold and a poly(ethylene) sheet was laminated to the mold and then slowly peeled away at a controlled rate. The filled mold was then placed face-down on the substrate; constant pressure was applied to the mold and the entire assembly was held at an elevated temperature to undergo the sol–gel transition via solvent removal, which is assisted by the air-permeable mold.[25] To obtain an embossed film (Figure $1c_2$–e_2), the liquid sol was drop-cast onto the substrate and the mold was pressed down and held at constant pressure. The sample was then held at an elevated temperature in order to undergo the

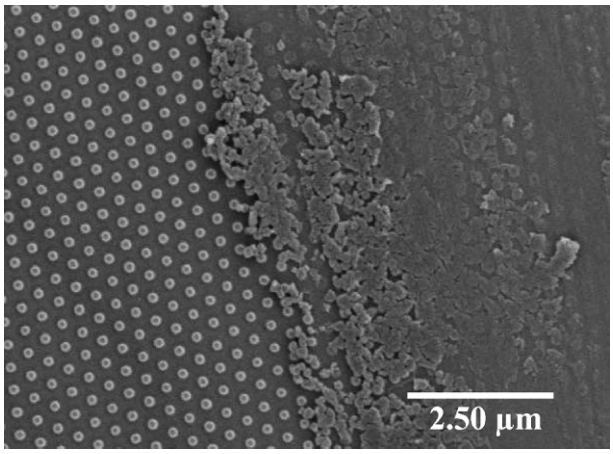

Figure 2. SEM image of an array of isolated anatase TiO_2 features. The pattern has been scraped with a doctor's blade to demonstrate the absence of an interconnecting flash layer between the features.

sol–gel transition. In both situations, the low-surface-energy PFPE mold was peeled off the substrate leaving either isolated xerogel features or an embossed xerogel film, as shown in Figure 1.

Once in the xerogel state, the substrate is calcined to form the desired crystalline phases. In the case of patterning TiO_2, the anatase phase is preferred because of its potential use in photocatalysis applications.[26] The topography and morphology of the resulting structures were analyzed by atomic force microscopy (AFM) and scanning electron microscopy (SEM).

Figure 2 is a SEM image of an array of isolated anatase titania features, which have been patterned on a glass substrate using the procedures outlined in Figure $1a$–e_1. In order to demonstrate the formation of an isolated array of features, a doctor's blade was used to scrape the surface of the substrate.

Figure 3 is a SEM image of an embossed array of patterned anatase TiO_2 replicated from a silicon master template consisting of a hexagonally patterned array of cylindrical posts, each 200 nm in diameter and 200 nm in height. Transmission electron microscopy (TEM) shows that the resulting anatase morphology consisted of crystallites that were approximately 10 nm in dimension.

In order to obtain these patterned titania features, traditional sol–gel chemistry techniques have been employed. To prepare a stable TiO_2 sol, the inorganic precursor titanium tetrakis(*n*-butyloxide), $Ti(OCH_2CH_2CH_2CH_3)_4$, was chelated with acetylacetone. This solution was diluted with 2-propanol before adding acetic acid as a catalyst. Upon solvent removal at 110 °C, a xerogel was formed. This amorphous solid was calcined at 450 °C to obtain the anatase form of crystalline TiO_2.[24] The characteristic powder X-ray diffraction (XRD) pattern of the bulk powder harvested after calcination of sol **1** (see Table 1) is shown in Figure 4.

Quantitative analysis of SEM results of the silicon master, PFPE mold, and TiO_2 replicas confirmed the high fidelity of the

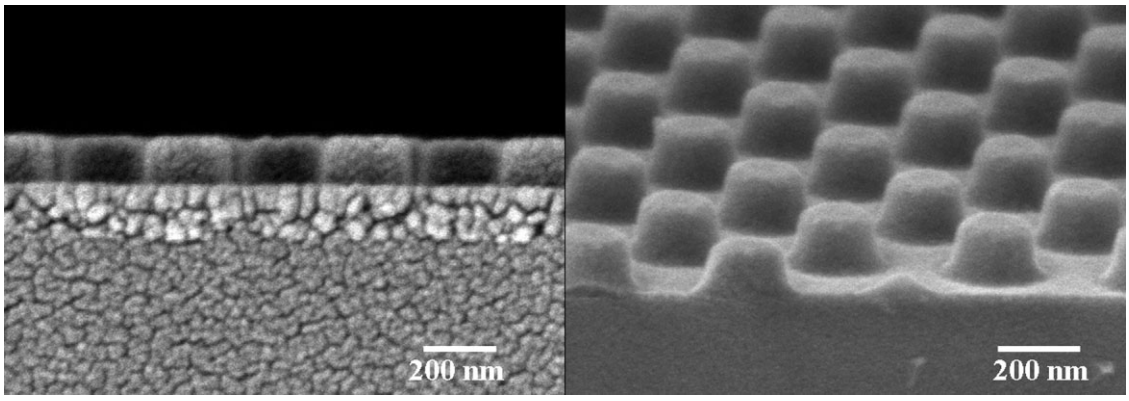

Figure 3. SEM image of anatase TiO_2 features on glass; the features are replicated from a silicon master with cylinders that are 200 nm in height and 200 nm in diameter.

PRINT process. Figure 5 shows the orientational order parameter $S = \frac{1}{2} < 3\boldsymbol{l}_i \cdot \boldsymbol{l}_j - 1 >$, where $\boldsymbol{l}_i$ and $\boldsymbol{l}_j$ are vectors between adjacent lattice sites along a given lattice direction **l** separated by a distance $|\boldsymbol{l}_i - \boldsymbol{l}_j|$; the brackets $\langle\rangle$ indicate an average over all pairs of vectors. [27] For a perfect hexagonal lattice, $S = 1.0$ independent of the separation between vectors; $S = 0$ for a disordered lattice. The master, mold, and replica had a value of unity within the experimental uncertainty for nearest neighbors; the order parameter in the titania pattern decayed slightly more rapidly with the separation distance relative to S for the master template and the PFPE mold. The basic conclusion from the image analysis was that the PRINT orientational order in patterned inorganic oxides was maintained over multiple lattice distances.

SEM images of patterned substrates before calcination are shown in Figure 6A and 6B, while images of patterned subtrates after calcination are shown in Figure 6C and 6D. The width and height of the xerogel features closely approximate the mold size, indicating good filling of the mold and a porous, amorphous network. After calcination, both the width and height of the features decreased; however, shrinkage along the z-axis was more significant. This anisotropic volume loss has also been observed in other work.[19,20]

Shrinkage of titania features after calcination was expected because of the low weight percentage of solids in the sol formulation. However, this volume loss can be minimized through modification of the sol recipe. Recipes for the sols used are given in Table 1. Sol **2** contained 13.3 wt% Ti and sol **1** 6.0 wt% Ti. Features patterned with sol **2** using a 200 nm × 200 nm mold exhibited approximately a 30% reduction in volume loss in comparison to features patterned with sol **1**. These results are summarized in Table 2.

In order to obtain high-fidelity patterns over large surface areas, volume loss must be minimized. Significant shrinkage after calcination can lead to loss of pattern details and severe cracking. By altering the sol–gel chemistry, it is possible to control the extent of feature reduction upon calcination.

Table 1. Molar equivalents for the titania sol formulations.

Sol	$Ti(OBu)_4$	Acetyl-acetone	Acetic acid	2-Propanol	Ti [wt.%]
1	6.7	15.6	1.0	20.0	6.0
2	20.0	2.0	1.0	2.0	13.3

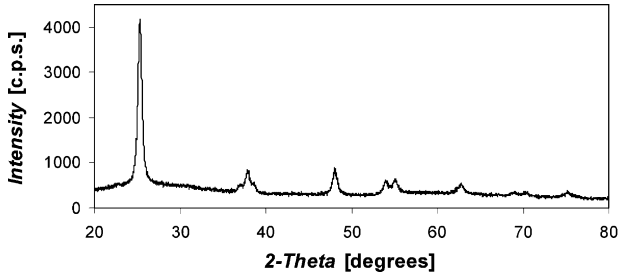

Figure 4. XRD spectrum of TiO_2 from a sample of the bulk sol–gel powder.

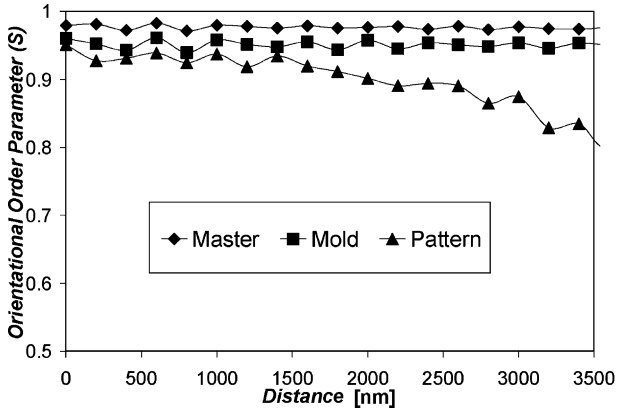

Figure 5. Orientational order parameter for a 200 nm × 200 nm Si master template, PFPE mold, and anatase TiO_2 pattern.

ADVANCED MATERIALS

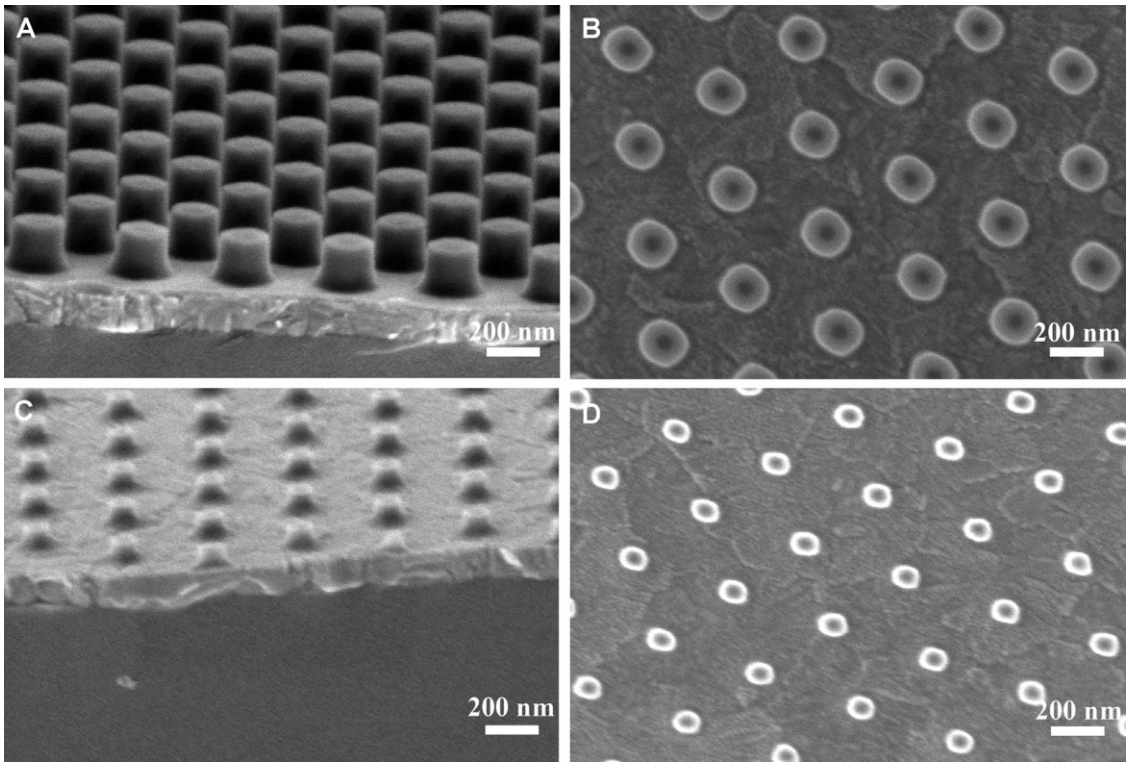

Figure 6. SEM images of an array of isolated titania features on an ITO-coated glass slide from a 200 nm × 200 nm mold using sol **1**. Images (A) and (B) are from the xerogel and images (C) and (D) were taken after calcination to form the anatase titania patterns.

Due to the nature of the patterning process and the extremely low surface energy of the PFPE elastomer utilized in PRINT, the substrate onto which patterns are created can be varied. Shown in Figure 7 are SEM images of titania features embossed onto glass, indium tin oxide (ITO)-coated glass, and fluorine tin oxide (FTO)-coated glass. Apparently the substrates used have little affect upon the ability of the PFPE mold to form a pattern using the sol–gel route. It can be seen from Figure 7 that all of the patterns shown have flash layers of various thicknesses. In photovoltaic applications, a flash layer is needed in order to prevent contact between two electrodes in a layered device configuration. In other applications a flash layer is not desired; however, the PRINT molding process is sufficiently flexible to be used in both situations.[12,15]

Other important aspects of PRINT are the ability to pattern various shapes, sizes, multiple layers, and a host of different materials. Pattern replication is not limited to structures with an aspect ratio of one. Silicon masters with cylindrical posts that were 200 nm in diameter and 600 nm in height were molded and replicated in titania, as shown in Figure 8. Due to lateral shrinkage, the anatase TiO_2 posts had an aspect ratio of approximately 2.5.

Table 2. Comparison of the shrinkage and volume loss in titania features after calcination. The characterization data were obtained from SEM measurements.

Sol	*x-y* Shrinkage [%]	*z*-axis Shrinkage [%]	Volume loss [%]
1	57	66	94
2	14	50	63

One significant advantage of soft lithography over hard imprint methods is the ability to deposit multiple layers without destroying the pattern of the first layer. An example of the inherent flexibility of the mold in soft lithography is shown in Figure 9, where a second generation of titania posts were patterned on top of the first generation. The intriguing pattern generated by the double PRINT process is a Moiré pattern, which results from the imperfect orientational alignment of two hexagonally patterned arrays of features. The double PRINT technique offers the potential to increase both the height and density of features without having to fabricate an expensive new silicon master.

The chemical resistivity of the PFPE mold is not limited to patterning of TiO_2 sols. A wide range of metal oxides can be obtained and subsequently patterned from sol–gel precursors. SnO_2, a transparent semiconductor, has recently been investigated for optoelectronics, hybrid microelectronics, and solar-energy conversion applications.[17] Many of these applications would benefit from the ability to pattern regular arrays of SnO_2 particles over a large surface area. Using a tin chloride

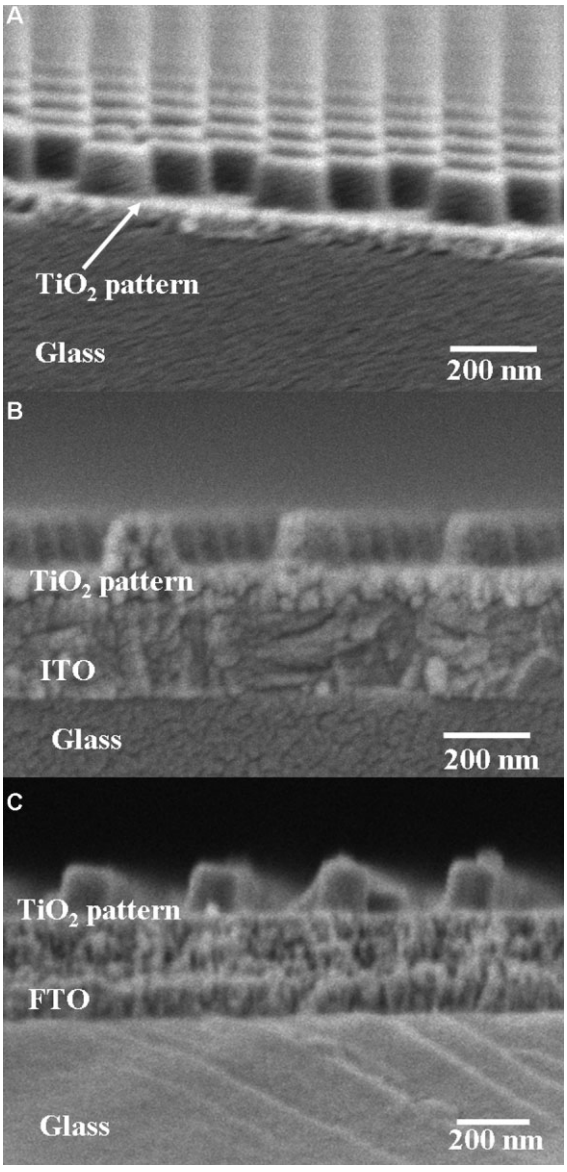

Figure 7. SEM image of anatase TiO_2 features replicated on (A) glass, (B) ITO-coated glass, and (C) FTO-coated glass.

precursor, a SnO_2 sol was obtained and used for patterning. Arrays of SnO_2 features generated from a 200 nm ×200 nm mold are shown in Figure 10A.

ZnO is a stable, wide-bandgap semiconductor with good electrical conductivity. Various devices employ thin films of ZnO such as piezoelectric transducers, solar cells, and gas sensors.[16] In particular, improved performance in solar cell and gas sensor applications could be achieved if highly ordered arrays of ZnO features could be fabricated. A ZnO sol was obtained using a zinc acetate precursor, and features were generated from a 200 nm × 200 nm mold, shown in Figure 10B. Unlike the TiO_2 and SnO_2 features, these patterns were not sharply defined. This sol formulation contained diethanolamine (DEA), which has a boiling point that is above the drying

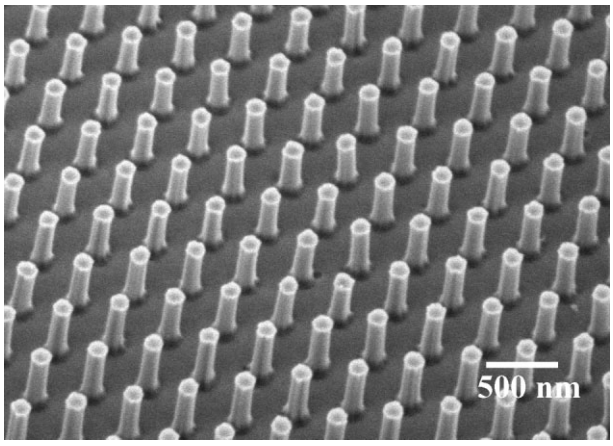

Figure 8. SEM image of TiO_2 features replicated from a 200 nm ×600 nm master.

temperature of the oven. The residual solvent may account for the deformed features observed in Figure 10B.

Indium tin oxide (ITO) is commonly used as a transparent conductor in electronic, optoelectronic, and mechanical applications, such as window heaters, solar cells, and liquid-crystal displays.[28] ITO features were patterned using a sol derived from indium nitrate and tin chloride precursors; the results are shown in Figure 10C.

Barium titanate is a ferroelectric ceramic that is commonly used for its dielectric, piezoelectric, and optical properties. It is used extensively as the filler component in polymer–ceramic composites. The ability to control the shape, orientation and size of dielectric heterostructures is of paramount importance to applications such as sensors, current limiters, acoustic actuators, microwave absorbers,[13] and the fabrication of photonic bandgap structures.[29] The $BaTiO_3$ features shown in Figure 10D were patterned from a barium acetate and titanium isopropoxide-based sol using a 200 nm × 200 nm PFPE mold.

In summary, the use of the PRINT technique has been extended to the patterning of sub-500 nm sized isolated

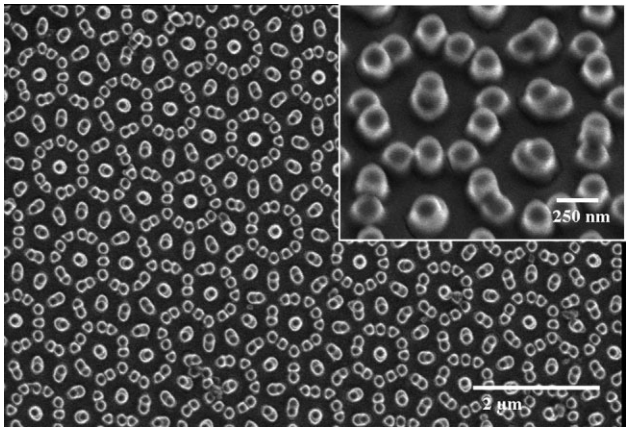

Figure 9. SEM image of a double-stamped TiO_2 pattern from a 200 nm ×200 nm mold. Inset image taken at a 30° tilt.

ADVANCED MATERIALS

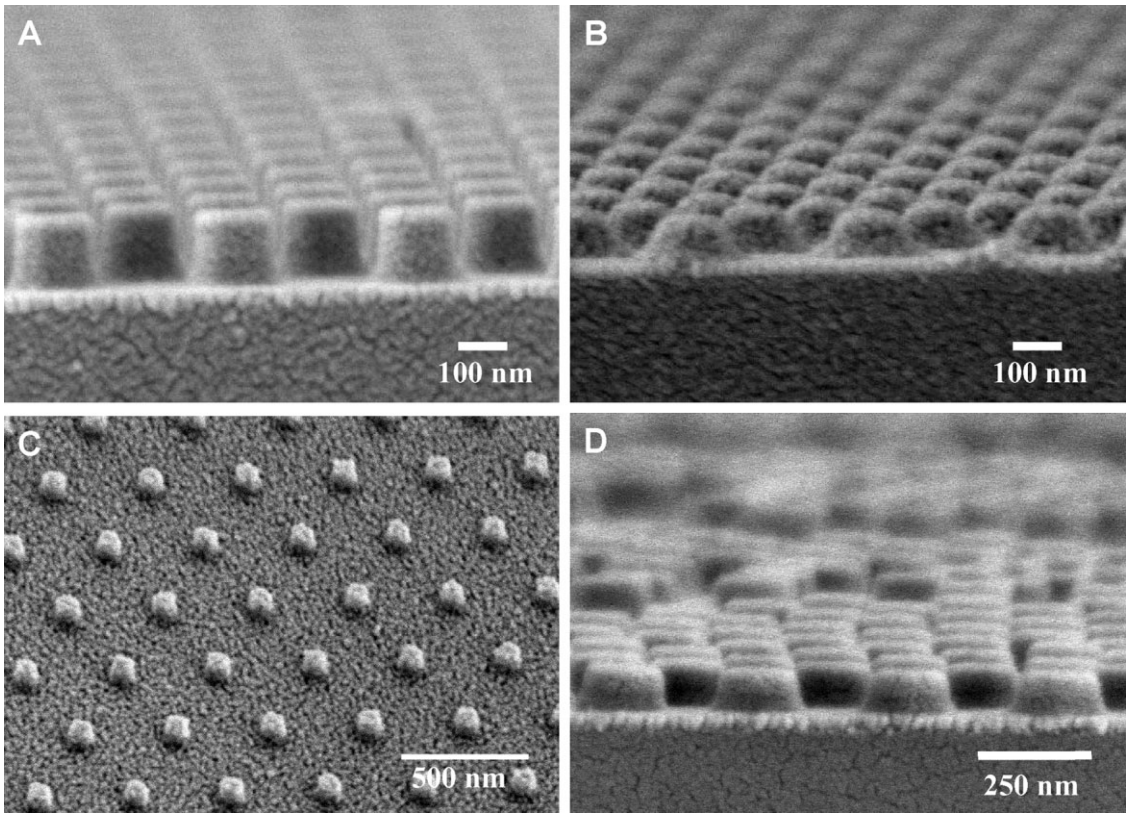

Figure 10. SEM images of arrays of various inorganic oxide features on glass made from a 200 nm × 200 nm mold: (A) SnO_2; (B) ZnO; (C) ITO; (D) $BaTiO_3$.

features as well as embossed films of inorganic oxides including TiO_2, SnO_2, ZnO, ITO, and $BaTiO_3$. The versatility of this soft lithography method allows patterns to be generated on a variety of substrates including glass and transparent conductive oxides. Volume loss upon calcination was observed for all sol–gel formulations; the extent of shrinkage can be controlled through adjustment of the sol chemistry conditions. PRINT provides a route for (1) patterning features with an aspect ratio larger than one and (2) layer-by-layer deposition without destruction of the first layer. Future work will target pattern replication on the sub-100 nm scale for microelectronic applications.

Experimental

To prepare titania sol **1**, titanium butoxide (10.0 g, 29.4 mmol) was mixed with acetylacetone (6.80 g, 68.0 mmol). After 15 min of stirring, the solvent 2-propanol (8.0 mL) was added to the solution. Glacial acetic acid (0.252 g, 4.19 mmol) was added dropwise to the stirring solution. The sol was stirred for 1 h and filtered with a 0.45 μm filter before use. To prepare titania sol **2**, the same procedure as above was followed, but with different molar ratios: $Ti(OBu)_4$ (9.0 g, 26.4 mmol), acetylacetone (0.262 g, 2.62 mmol), 2-propanol (0.20 mL), and glacial acetic acid (0.079 g, 1.31 mmol). To convert TiO_2 into the anatase form, samples were heated to 450 °C at a rate of 10 °C per min and held at 450 °C for 30 min.

To prepare the SnO_2 sol, $SnCl_2 \cdot 2H_20$ (3.82 g, 16.9 mmol) was dissolved in anhydrous ethanol (37.5 mL). This solution was refluxed at 80 °C for 2 h, allowed to cool to room temperature, and then filtered with a 0.45 μm filter before use. In order to obtain crystalline SnO_2, samples were heated to 450 °C at a rate of 10 °C per min and then held at 450 °C for 30 min.

To make the ZnO sol, zinc acetate dihydrate (2.20 g, 10.0 mmol) was dissolved in 2-propanol (10 mL). Diethanolamine (1.05 g, 10.0 mmol) was added rapidly to the stirring solution. The solution was heated to 50 °C and after 10 min deionized water (0.09 mL) was added dropwise. The solution was allowed to cool to room temperature and was then filtered with a 0.45 μm filter before use. In order to obtain crystalline ZnO, samples were heated to 500 °C at a rate of 10 °C per min and held at 500 °C for 1 h.

To prepare the sol precursor of ITO, indium nitrate pentahydrate (2.05 g, 5.24 mmol), tin cloride pentathydrate (0.15 g, 0.428 mmol), acetylacetone (3.16 g, 31.6 mmol), and water (0.009 mL) were mixed in one vial and stirred at 50 °C for 2 h. In another vial, benzoylacetone (0.851 g, 5.25 mmol) and 2-methoxyethanol (20.7 mL) were added and allowed to stir at room temperature for 2 h. The solutions in the two vials were combined and allowed to stir at room temperature for at least 8 h before use. To convert ITO into the crystalline form, samples were heated to 600 °C at a rate of 10 °C per min and held at 600 °C for 1 h.

To make the $BaTiO_3$ sol, a 42 wt.% barium acetate solution in glacial acetic acid was prepared by dissolving barium acetate (0.382 g, 1.50 mmol) at 85 °C. The sample was cooled to 50 °C and titanium(IV) isopropoxide (0.417 g, 1.47 mmol) was added. The solution was diluted with 2-methoxyethanol (0.1 mL) and filtered through a 0.45 μm PTFE filter. In order to obtain crystalline BaTiO3, samples were heated to 700 °C at a rate of 10 °C per min and held at 700 °C for 1 h.

All materials were purchased from Aldrich and used as received. All metal oxides were characterized with an X-ray diffractometer (XRD, Rigaku) using Cu Kα radiation. SEM images were obtained with a Hitachi S-4700 instrument.

Received: October 4, 2007
Published online: June 2, 2008

[1] Y. Xia, J. A. Rogers, K. E. Paul, G. M. Whitesides, *Chem. Rev.* **1999**, *99*, 1823.
[2] S. Y. Chou, P. R. Drauss, P. J. Renstrom, *Science* **1996**, *277*, 85.
[3] B. D. Gates, O. Xu, M. Stewart, D. Ryah, C. G. Willson, G. M. Whitesides, *Chem. Rev.* **2005**, *105*, 1171.
[4] Y. Xia, G. M. Whitesides, *Angew. Chem. Int. Ed.* **1998**, *37*, 551.
[5] G. M. Whitesides, E. Ostuni, S. Takayama, X. Jiang, D. E. Ingber, *Annu. Rev. Biomed. Eng.* **2001**, *3*, 335.
[6] J. P. Rolland, R. M. Van Dam, D. A. Schorzman, S. R. Quake, J. M. DeSimone, *J. Am. Chem. Soc.* **2004**, *126*, 2322.
[7] J. P. Rolland, E. C. Hagberg, G. M. Denison, K. R. Carter, J. M. DeSimone, *Angew. Chem. Int. Ed.* **2004**, *43*, 5796.
[8] T. T. Truong, R. Lin, S. Jeon, H. H. Lee, J. Maria, A. Gaur, F. Hua, I. Meinel, J. A. Rogers, *Langmuir* **2007**, *23*, 2898.
[9] L. E. Euliss, J. A. DuPont, S. Gratton, J. M. DeSimone, *Chem. Soc. Rev.* **2006**, *35*, 1095.
[10] J. P. Rolland, B. W. Maynor, L. E. Euliss, A. E. Exner, G. M. Denison, J. M. DeSimone, *J. Am. Chem. Soc.* **2005**, *127*, 10096.
[11] B. W. Maynor, I. LaRue, Z. Hu, J. P. Rolland, A. Pandya, Q. Fu, J. Liu, R. J. Spontak, S. S. Sheiko, R. J. Samulski, E. T. Samulski, J. M. DeSimone, *Small* **2007**, *3*, 845.
[12] C. Goh, K. M. Coakley, M. D. McGehee, *NanoLetters* **2005**, *5*, 1545.
[13] C. Brosseau, A. Beroual, A. Boudida, *J. Appl. Phys.* **2000**, *12*, 7278.
[14] S. Liu, A. Chen, *Langmuir* **2005**, *21*, 8409.
[15] P. Yang, M. Yang, S. Zou, J. Xie, W. Yang, *J. Am. Chem. Soc.* **2007**, *129*, 1541.
[16] P. Ravirajan, A. M. Peiro, M. K. Nazeeruddin, M. Graetzel, D. Bradley, J. R. Durrant, J. Nelson, *J. Phys. Chem. B.* **2006**, *110*, 7635.
[17] X. Ai, N. Anderson, J. Guo, J. Kowalik, L. M. Tolbert, T. Lian, *J. Phys. Chem. B.* **2006**, *110*, 259496.
[18] D. Xia, D. Li, Z. Ku, Y. Luo, S. J. Brueck, *Langmuir* **2007**, *23*, 5377.
[19] O. F. Gobel, M. Nedelcu, U. Steiner, *Adv. Mater.* **2007**, *17*, 1131.
[20] S. Seraji, Y. Wu, N. E. Jewell-Larson, M. J. Forbess, S. J. Limmer, T. P. Chou, G. Cao, *Adv. Mater.* **2000**, *12*, 1421.
[21] B. Su, D. Zhang, T. W. Button, *J. Mater. Sci.* **2002**, *37*, 3123.
[22] N. E. Voicu, M. M. Saifullah, K. V. Subramanian, M. E. Welland, U. Steiner, *Soft Mater.* **2007**, *3*, 554.
[23] P. Yang, T. Deng, D. Zhao, P. Feng, D. Pine, B. F. Chmelka, G. M. Whitesides, *Science* **1998**, *282*, 2244.
[24] B. D. Gates, Q. Xu, M. Stewart, D. Ryan, C. G. Willson, G. M. Whitesides, *Chem. Rev.* **2005**, *105*, 1171.
[25] C. J. Brinker, G. W. Scherer, *Sol–Gel Science: The Physics and Chemistry of Sol–Gel Processing*, Academic Press, San Diego, CA **1990**.
[26] A. L. Linsebigler, G. Lu, J. T. Yates, *Chem. Rev.* **1995**, *95*, 735.
[27] M. Rubinstein, D. R. Nelson, *Phys. Rev. B* **1982**, *26*, 6254.
[28] Y. Li, G. Zhao, W. Zhang, Y. Chen, *J. Display Technol.* **2006**, *2*, 175.
[29] S. Hirano, S. Shimade, M. Kuwabara, *Appl. Phys. A.* **2005**, *80*, 783.